

Magnus Wind Turbine Effect Vertical Axis Using Rotating Cylinder Blades

Khalideh Al bkoor Alrawashdeh*, Nabeel.S.Gharaibeh, Abdullah A. Alshorman,
Mohamad H. Okour

Mechanical Engineering Department, Al-Huson University College, Al-Balqa' Applied University, P.O.Box 50, Al-Huson, 19117 Irbid, Jordan.

Received July 17 2020

Accepted November 30 2020

Abstract

The aerodynamic characteristics of a Magnus wind turbine (MWT) with cylinder blades are evaluated by using numerical simulation COMSOL. Yaw and lifting systems are used to identify the features of the MWT to maximizing power output at minimum stresses, torque and fatigue. MWT is characterized by low efficiency of power production. Therefore, it is important to seek effective components to improve the power performance of MWT. The blades design in Yaw and lifting system are critical parameters that affect MWT performance. In this study, five suggestions were discussed to choose the best configurations of MWT in order to promote MWT application. Performance characteristics, such as stresses, Torque, deflection and fatigue with suggested configurations are analyzed and compared to identify the desirable components for this type of MWT. The results showed that the aerodynamic characteristics of MWT in this study will be presented as a significance guide for the initial research and preliminary design of MWT. Based on the suggested design configuration, the results showed that the Von Mises stresses are low at the bottom and high at the top, and the buckling is very high at the top but low at the bottom of the base while the maximum value of Findley's fatigue is for the bottom as a result of axial stress. As for the designed shaft, the force increases when the stress increases accordingly, therefore, the deflection also increases. Moreover, the results showed more specified ranges of stresses distributions on blades and deflection ranges of decrease and increase that enable for better design, control and power utilization of turbine.

© 2021 Jordan Journal of Mechanical and Industrial Engineering. All rights reserved

Keywords: Magnus effect, wind turbine, stress, deflection, torque, yaw system;

1. Introduction

The world today faces a continuous looming threat of limited resources and energy; the burning of fuel can no longer be viewed as the only means to obtain energy. Renewable (Khatri et al., 2010), safe and sustainable ways of generating energy must be developed, and it is always the responsibility of engineers to make that possible. The wind power plays an important role in tackling climate change, and that through new designs and concepts, it allows for greater yield and efficiency of energy in its application. Wind turbines (WT) have come a long way in a short period of time since their initial development in the 1970s; consumption of electricity of grid and its cost had fallen greatly (Kaygusuz, K., 2004).

The regular wind turbines need high wind speed, which is not available in the Middle East as the average wind speed is 5.5 m/s (Musgrove, p, 1993; Ahmeda and Mahammeda, 2012; Jinbo et al., 2015). Wind turbines take advantage of wind power by converting the kinetic energy to electrical energy (Lu, X et al., 2009; Messaoud and Abdessameda, 2011). Wind power has proven to be one of the most

efficient and economical sources. It is environmentally energy friendly (Fauzan et al., 2017).

Under the force of the wind, the blades will rotate around a horizontal or vertical axis, and this kinetic energy will drive the turbine to generate power (Benatiallah et al., 2010; Fredous et al., 2011, Ghenai, 2017; Messaoud et al., 2018). Electricity production depends on the speed of the airflow and blades design (Cox et al., 2017; AEO, 2017; Mishra et al., 2017). Wind turbines are manufactured in two local sizes, which are building - mounted and pole mounted (Kunz et al., 2007; WWEA, 2012; Minderman et al., 2012). Pole mounted turbines are free standing in a suitable position, generating 5 kW and more of electricity (Tangler, 1994, Schube et al., 2012). Building mounted turbines are small - sized, where it can be located on the roof and between buildings, and generate less power than the pole mounted turbines (Owens, 2014; Messaoud et al., 2018). Small turbines are used for applications such as charging a battery of a car, boat, caravans and to power traffic signs and for lighting small area like camps, parking and small fields.

The first MWT consisted of a brass cylinder fitted between two bearings and rotated at high speed using a string (Golding, 1976). The cylinder was attached to a freely

* Corresponding author e-mail: khalideh19@bau.edu.jo.

rotating arm and air from a blower was directed towards it (Seifert, 2012). As the Cylinder rotated, it was noticed that the spinning cylinder always tended to deflect towards the side of the rotor that was traveling in the same direction as the wind coming from the blower (Seifent. J, 2012; BORG, 1986). The idea of using the Magnus effect in many applications leads to develop a cylinder-blade windmill by coiling the spiral fins around the cylinders producing a spiral Magnus turbine (Sun et al., 2012). When the spiral cylinders catch the wind, the rotating force is generated due to the aerodynamic properties caused by Magnus Effect. The technologies of WT in conjunction with the Magnus effect has progressed greatly, in addition, electricity generation has risen almost exponentially.

The main objective of this study is to use the Magnus effect to rotate the blades at a lower airspeed. The suggested design utilizes wind energy and the Magnus effect as a lifting force on the circulating airfoil blade attached to a wind turbine design. The circulating airfoil shape is a new concept developed theoretically and will be implemented for the first time. The circulating airfoil design will be scaled to match that of a NACA0021 airfoil which shows high aerodynamic quality (Abbott and Doenhoff, 1959; Gregorck, 1989).

This study utilizes Magnus effect as a lifting force on circulating an airfoil blade attached to a wind turbine design. The circulating airfoil will rotate around its axis resulting in high pressure on a side while the other side will have low pressure which leads to lifting the rotor. The turbine is going to be portable where it can fit into small areas; such as small camping areas, small apartments, parking and a small park.

2. Modelling of MWT

The blade design will be the new circulating airfoil blade design consisting of two different sized cylinders, one of

which is connected to a DC motor to circulate the airfoil surface and the other one rotating freely and maintaining the airfoil shape as shown in figure 1a. The hub of the wind turbine will house the two DC motors connected to two circulating airfoil blades. Also, there will be a generator that is connected to the blade's shaft to change the rotation action to energy that will be stored in a battery.

The study reported in this paper examines, using numerical analyzed, the aerodynamic characteristics of a MWT with cylinder blades in Yaw and lifting system to identify the features of the MWT to maximizing power output at minimum stresses, torque and fatigue, in addition to the influences of deflection.

The block diagram in figure 1b shows how the MWT works. Initially, battery 1 will turn on the cylinders of the blades of the Magnus wind turbine. The wind will attack the blades applying high pressure on the side of the blade that is rotating in the opposite direction of the wind. While the other side will have low pressure since it is rotating in the same direction as the wind. Therefore, the net force will result in lifting the blades. Then the transformation of kinetic energy into electrical energy will be done by the generator, which is connected to the blades by a rotating shaft with a gearbox. The generator will defuse the electrical energy for three different purposes. The first one will be for charging battery 1, which is the response to turn on the yaw system, the lift system and the initialization system. The second purpose is to charge battery 2 until sunset and discharge the stored energy for lighting after that. The third one is to transfer direct electrical power to lighting. There will be an emergency manual braking system that is connected to the rotating shaft to shut down the machine when needed. Also, the blades can be turned on manually in case the battery is dead.

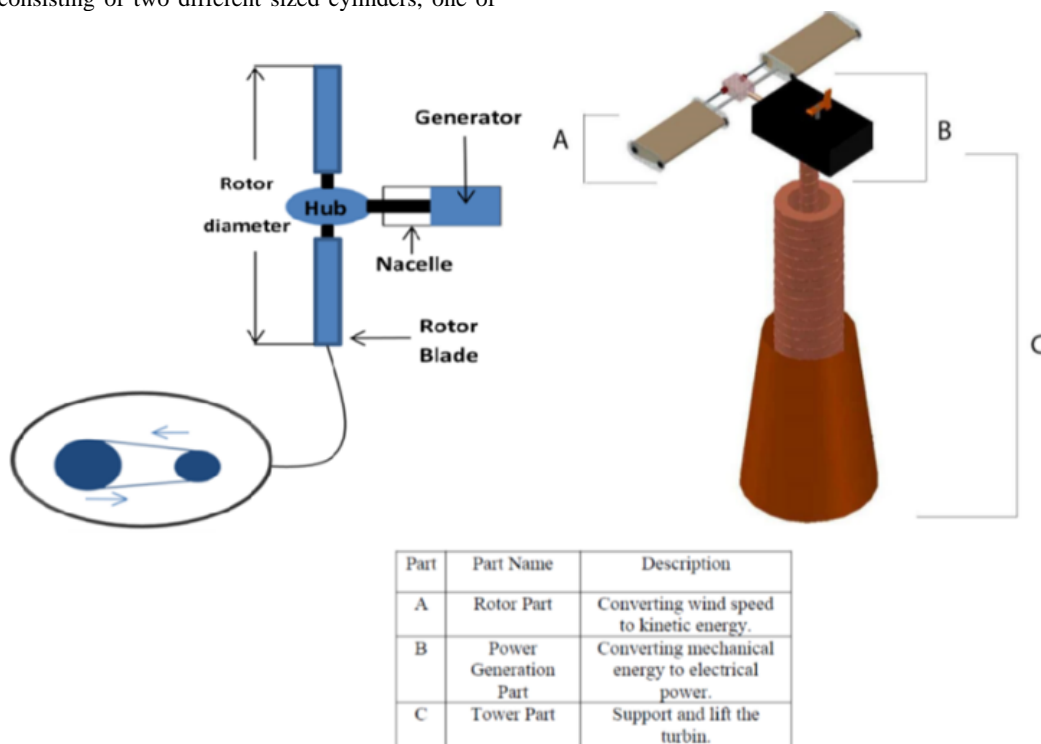


Figure.1a: The mechanism of the MWT

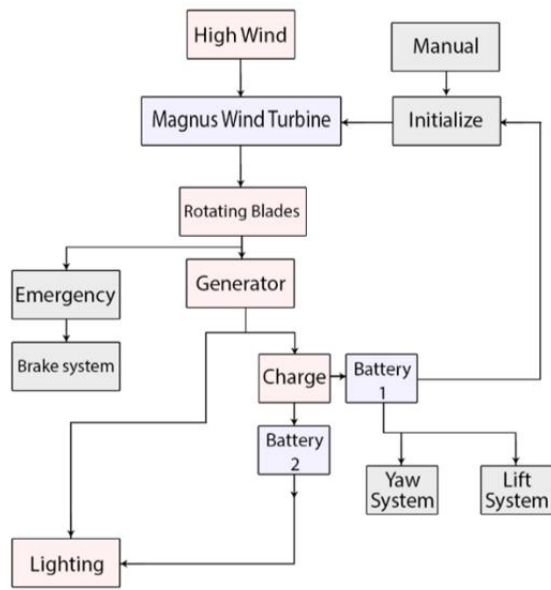


Figure.1b: The operation mechanism of the MWT

Figure 2 shows the rotation part of the blades (A), the power generator part –Nacelle (B). Table 1a shows the entire components of part A with the description, material, and manufacturing process. This part of the MWT consists of two blades; each one consists of two cylinders, two holders and a shaft that is connected to the motors through the coupler. The hub connects the blades to the low-speed shaft that is connected to the gearbox. The low-speed shaft will pass through a ball bearing that will be installed inside the hub to reduce the friction and to rotate the shaft smoothly.

In part B, the two shafts in this part are the high-speed shaft which will help to generate electricity and the other shaft is the lower speed shaft which is connected to the blades through the hub. The chokes are attached to the low speed shaft to support and keep it stable. The microcontroller, the indicator, and the yaw motor are representing the yawing system that rotates the turbine to face the wind’s direction. A generator is attached to the high-speed shaft to generate power. The braking system is attached to the low-speed shaft for the emergency stop.

Finally, the gearbox is used to transmit the rotation of the low-speed shaft to the high-speed shaft to generate power from the generator. Table1b shows the entire components with the description, material, and the manufacturing process.

Table.1a: Components of part A of MWT.

Part #	Part Name	description	Material	Manufacturing process
1	Large Blade's Shafts	Rotate blades	Aluminum	Purchased
2	Small Blade's cylinders	Rotate blades	Aluminum	Purchased
3	Hub	Keep shafts stable	Aluminum	Purchased
4	Ball Bearings	Smooth rotation	Aluminum	Purchased
5	Blade's Edges	Keeps cylinders in place	Rubber	Purchased
6	Stationary Shafts	Support the blade	Aluminum	Manufactured
7	Belt	Airfoil shape	Aluminum	Manufactured
8	Motors	Magnus effect	Aluminum	Manufactured
9	Rotating Shafts	Rotate the large shaft	Aluminum	Purchased

Table. 1b: Components of part B of MWT

Part #	Part Name	Description	Material	Manufacturing process
1	Choke	Keep shafts stable	Aluminum	Purchased
2	Low Speed Shaft	Transmit blade's rotation	Aluminum	Purchased
3	Brake System	Stops rotation of rotor	-	Purchased
4	Generator	Generate power	-	Purchased
5	Indicator	Wind direction indicator	Plastic	Purchased
6	Nacelle	Protects and covers the items	Aluminum	Manufactured
7	Yaw motor	Rotate the rotor	Aluminum	Purchased
8	High Speed Shaft	Connects gearbox to generator	Aluminum	Purchased
9	Pins	Enclose nacelle	-	Purchased
10	Microcontroller	Sends signal to yaw motor	Aluminum	Purchased
11	Gearbox	1:15 increasing rpm	Aluminum	Purchased

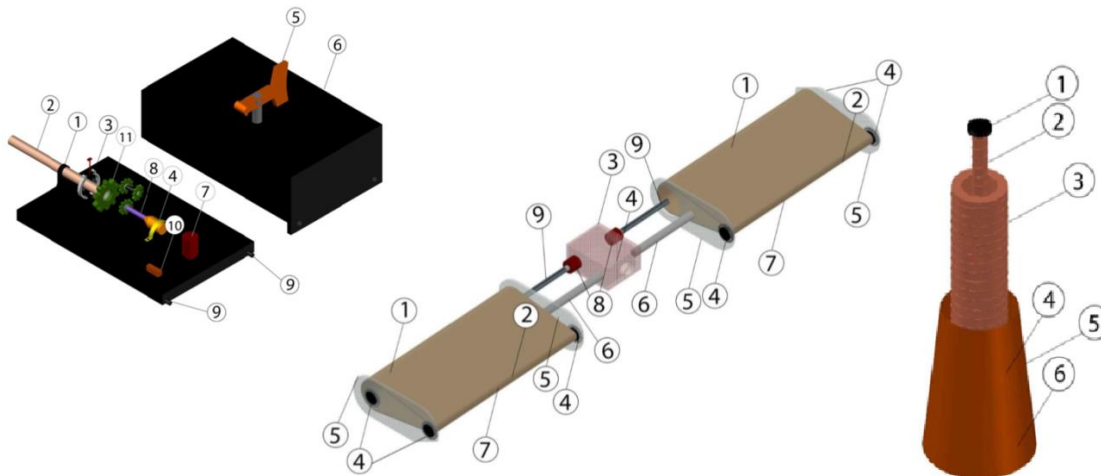


Figure. 2: Part A, B and C of the MWT assembled.

The lower body of the Magnus wind turbine is shown in Figure 2. The tower contains three parts: the base and two power screwed towers for lifting, also in the tower the bevel gear is shown inside the base of it for lifting the tower to the maximum height. The batteries of the turbine are hidden in the base of the tower, where one of the batteries is used for the yawing and lifting system, while the other battery is for lightning. Finally, the gear is installed at the top of the tower for the yawing system. Table 1c shows the entire components with the description, material, and manufacturing process.

Table. 1c: Component of part C of MWT

Part #	Part Name	Description	Material	Manufacturing process
1	Spur Gear	Yaw system	Aluminum	Purchased
2	Tower C	Power screwed Tower	Aluminum	Purchased
3	Tower B	Power screwed Tower	Aluminum	Purchased
4	Tower A	Base of Tower	Aluminum	Manufactured
5	Batteries	For initializing and - charging		Purchased
6	Bevel Gears	For lifting system	Aluminum	Purchased

2.1. Design Proposal:

The MWT is divided into three main parts as shown in Figure 1, each part has different components. Some components need to be analyzed to avoid failures. Some components will be analyzed by calculations, while other parts will be numerically analyzed. The structural numerical analysis will be applied on stationary shafts that are connected between the hub and the airfoil blades to determine the stress, deflection and fatigue.

- The structural numerical analysis will be applied to the low-speed shaft to find stress, fatigue, deflection, and vibration.

- The structural numerical analysis will be applied to the towers to determine the stress, fatigue, buckling and deflection.

- Blades Analysis:

The first thing to start with is the blade's dimensions since they are the most important thing in the MWT. For rotating cylinder dimensions, assuming that: Airfoil shape of NACA 0021, the Speed ratio of $\alpha=1$ and the Rated wind speed, $V_{wind}=15$ m/s. Applying the speed ratio equation first to get the radius of the front cylinder of the blade:

$$\alpha = V_{Magnus} / V_{Wind} \quad (1)$$

$$\alpha = (\omega \times R_{cylinder}) / V_{wind} \quad (2)$$

The radius of rotating cylinder equal to:

$$R_{cylinder} = 0.06 \text{ (m)}$$

The diameter of rotating cylinder equal to:

$$D_{cylinder} = 2 \times R_{cylinder} \quad (3)$$

$$D_{cylinder} = 0.12 \text{ (m)}$$

The diameter of the front circle is almost considered to be equal to 21% of the rare diameter to make an approximate similarity to NACA0021. Diameter of rare cylinder:

$$D_{Rare \ cylinder} = 0.21 \times D_{Front \ cylinder} \quad (4)$$

$$D_{Rare \ cylinder} \approx 0.03 \text{ (m)}$$

Assume chord length to be 0.35 m.

For Rotor length assume the Coefficient of Power (C_p) =0.3, Density of Air (ρ)=1.225, Output Power (P) =1000 Watts and the Rated wind speed (V_{wind}) =15 m/s. Using power equation to measure rotor radius:

$$P = 0.5 \times \rho \times A \times V^3 \times C_p \quad (5)$$

Therefore, the rotor radius will be $R_{rotor}=0.75$ (m) by using equation 5.

For the stationary blade shaft Analysis: Stress analysis will be made to get the diameter of the shaft that connects the hub to the blades and supports them. Assume the Length (L)=0.24 m, Factor of Safety (n) =4, and Yield Strength (σ_y)=169 MPa.

$$n = \sigma_y / \sigma_{allowable} \quad (6)$$

$$\sigma_{allowable} = (M \times C) / I \quad (7)$$

Using equations 6 and 7, the minimum diameter that can be used is equal to $d = 0.02$ m. The chosen diameter, $d=0.03$ m. To analyze the low speed shaft stress (see Figure 3), the structural analysis will be applied to determine the diameter of the low speed shaft that connects the blades to the gearbox. By assuming the following: Length (L) =0.5 m, Factor of Safety (n) =4. 3 and the Yield Strength (σ_y) =169 MPa.

Determine the allowable stress to get the minimum diameter for the shaft by using equation 6 an 7, then the $d = 0.03$, so the chosen diameter $d=0.04$ m.

- Deflection Analysis

Structural analysis is applied to verify the deflection. Deflection analysis will help to know whether the material will handle the load or fail. In the case of Defection at blades, the length, height and width of each blade are given by 1.05, 0.17 and 0.4 m, respectively. Assuming the blades cantilever beam and has modulus of elasticity $E=71.9$ GPa. Then, the deflection can be found by:

$$\delta = R \times L \times E \times I \quad (8)$$

$$\delta = 1 \times 10^{-5} \text{ m}$$

While in the case of deflection at Tip of low speed shaft, the length, mass and diameter of each blade is given by 0.1 m, 1.7 kg and 0.04 m, respectively. Assuming the blades cantilever beam and has modulus of elasticity $E=71.9$ GPa. Then, the deflection can be found by deflection (Eq. 8), therefore the $\delta = 1 \times 10^{-6}$.

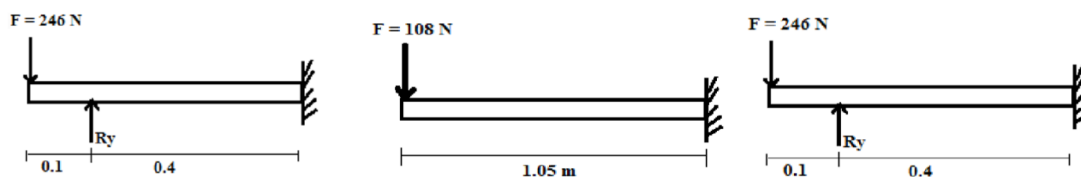


Figure. 3: Free body diagram of a. the low speed shaft, b. the stationary shaft and c. the Low speed shaft

- Vibration analysis

This analysis will help to determine whether there will be whirling in the low speed shaft or not. By Assuming: Eccentricity (a) = 2×10^{-3} m, Mass (m) = 1.7 kg, Angular velocity (ω) = 30 rpm, Length (l) = 0.5 m and Diameter (d) = 0.04 m.

$$\text{Stiffness } (k) = (48 \times E \times I) / L^3 \tag{9}$$

$$\text{Natural frequency } (\omega_n) = (k/m)^{0.5} \tag{10}$$

$$\text{Frequency Ratio } (r) = \omega / \omega_n \tag{11}$$

$$\text{Amplitude } (A) = (\alpha \times r^2) / (1 - r^2) \tag{12}$$

Substituting and solving equations 9, 10, 11 and 12, $A = 6.27 \times 10^{-8}$ m. Therefore, there is no whirling in this shaft.

- Gearbox Analysis

Gearing analysis is applied to determine number of teeth and diameter of each gear. By assuming Gearbox ratio 15:1, Minimum number of teeth to avoid interference (N) = 16, Pressure angle (Θ) = 14.5 and Module (m) = 2 mm. Since the gearbox ratio is 1:15, the ratio of number of teeth can be taken as: $N_2/N_3 = 5$ and $N_4/N_5 = 3$ (see figure 4). So, $N_2 = 5 \times N_3 = 5 \times 16 = 80$ teeth, $N_4 = 3 \times N_5 = 3 \times 16 = 48$ teeth. Then diameter of each gear was can be determined by equation 13, so, the $D_3 = 32$ mm, $D_2 = 160$ mm, $D_4 = 96$ mm.

$$D = m \times N \tag{13}$$

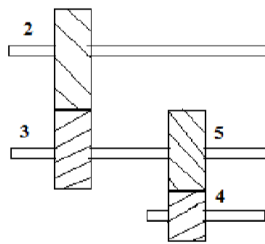


Figure. 4: Free Body Diagram of the Gearbox.

- High Speed Shaft Analysis

Lift Force can be calculated by equation 14, by Assuming the Rated wind speed, $V_{wind} = 15$ m/s, Lift Coefficient, $CL = 1.2$ and out power, $P = 1000$ watt

$$\text{Lift force equation } (L) = 1/2 \times C_L \times \rho \times A \times v^2 \tag{14}$$

$$\text{Torque equation } (T) = L \times 1/3 \times R_{rotor} \times n \tag{15}$$

$$\text{power equation } (P) = T \times \omega \tag{16}$$

Substituting all the variables, the lift force $L = 43.41$ N, the torque $T = 21.705$ N.m and $\omega = 440$ rpm.

The structural analysis will be applied to determine the diameter of the high-speed shaft that connects the gearbox

to the generator. Assuming, Torque (T) = 21.705 N.m, Factor of Safety (n) = 4.3, Yield Strength (σ_y) = 169 MPa, Length (l) = 0.12 m and Pressure angle (Θ) = 14.5.

$$\text{Tangential force } (F_{tang}) = T / R_{gear} \tag{17}$$

$$\text{Normal force } (F_n) = F_{tang} \times \tan 14.5 \tag{18}$$

$$\text{Moment equation } (M) = F_{normal} \times L \tag{19}$$

Substituting and solving equations 6, 7, 17, 18 and 19, the minimum diameter that can be used is equal to $d = 0.015$. Then the chosen diameter $d = 0.02$ m.

3. Result: Numerical Analysis (CAD)

In this section, numerical analysis was applied to the low speed shaft, stationary shaft, and the tower using COMSOL, (COMSOL Multiphysics software, this software is an interactive environment for modeling and simulating scientific and engineering problems and applications). The studies on these parts were Solid mechanics studies using the Von Mises failure theory (Wenchao et al., 2016; Rao et al., 2016), and Findley's fatigue studies were applied to determine the fatigue of the first study. The materials used on all of these parts are assumed to be aluminum in COMSOL, and the properties assumed for the aluminum are shown in the table below.

Table. 2: Properties used for COMSOL

Property	Value	Unit
Density	2700	Kg/m^3
Young's modulus	70×10^9	Pa
Poisson's ratio	0.33	--
Findley's stress sensitivity coefficient	0.2	--
Findley's limit factor	213×10^6	Pa
Matake's stress sensitivity coefficient	0.27	--
Matake's limit factor	223×10^6	Pa

The tower is divided into three parts, where it is assumed that it is fixed at the bottom while it has an axial force at the top for each part. The boundary conditions are fixed constraint at the bottom of each part and a boundary load at the top of each part of the tower. For the upper part of the tower, it is shown in figure 5 that the Von Mises stresses and the buckling are moderately high. This agrees with the results of another study conducted by Genzalez et al (2011), they showed that The Von Mises criterion is a good option for ductile materials with equal tensile and compressive strength, which is coincident with Von Mises for non-ductile materials.

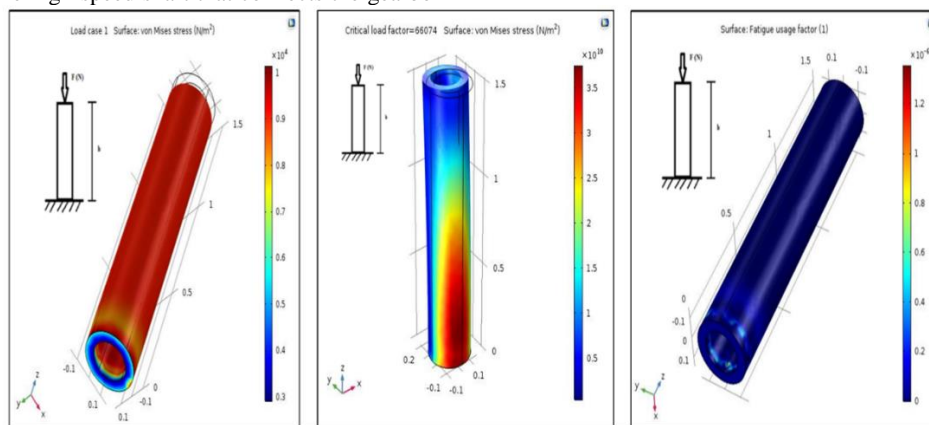


Figure. 5: a. Stress at the upper tower, b. Buckling in the upper tower and c. Fatigue in the upper tower

The fatigue analysis boundary conditions were taken from the studies of solid mechanics (see figure 5c). It is shown that the Findley's fatigue of the upper part of the tower is very low. The maximum fatigue of this part occurred at the bottom, consistent with the analysis study conducted by Li. H et al., (2018), that the fatigue damage relates much with the axial stress of the tower base, and under higher wind speed, the tower base experiences higher fatigue damage.

For the middle part of the tower, the boundary conditions are fixed constraint at the bottom of this part and a boundary load at the top of this part of the tower. It is shown in figure 6 that the Von Mises stresses and the buckling is moderately high, that corresponding with Chantharasenawong et al., (2011), that an Increasing in base diameter, not reflected in lower tower mass but also improves the stability of

structures with a higher natural frequency of tower and lower maximum tip deflection.

As shown in figure 6, the fatigue analysis boundary conditions were taken from the studies of solid mechanics. It is shown that Findley's fatigue in the middle part of the tower is very low. The maximum fatigue of this part occurred at the bottom. Also, the fatigue in this part is less than the fatigue of the upper part of the tower.

Finally, the base of the tower the Von Mises stresses are different from the previous two parts. The boundary conditions are fixed constraint at the bottom of this part and a boundary load at the top of this part of the tower. It is shown in figure 7 the Von Mises stresses are low at the bottom while high at the top, and the buckling is very high at the top while it is low at the bottom of the base.

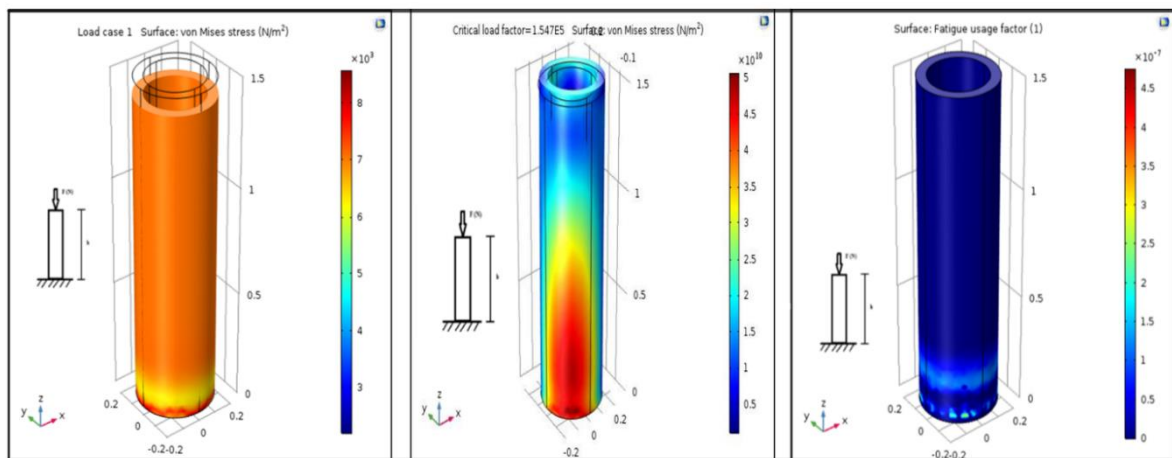


Figure 6: a. Stress in middle tower, b. Buckling of the middle tower and c. Fatigue in the middle tower

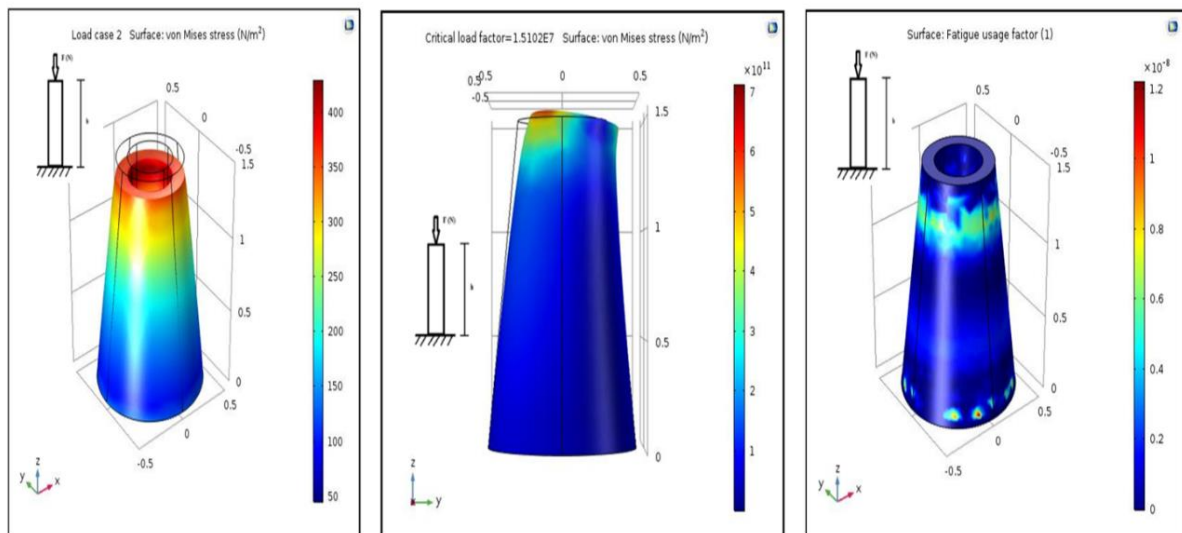


Figure 7: a. Stress at the tower base, b. Buckling at the tower base and c. Fatigue in the tower base

The fatigue analysis boundary conditions were taken from the studies of solid mechanics (see figure 7c). It is shown that Findley's fatigue of the base part of the tower is moderately low. The maximum fatigue of this part occurred at the bottom. Also, the fatigue in this part is less than the fatigue of the upper part of the tower, this is related to the dimensions, geometry and material of the tower in addition to the dynamic cyclic loading of wind speed and motion.

The numerical analysis of the low-speed shaft in COMSOL is shown below where the shaft was assumed to be a simple design problem of a fixed beam that has a force at the end and torque. The boundary conditions of the low-speed shaft are a fixed constraint on the left side of the shaft, a point load on the top right side of the shaft, and a rotating frame with a speed of 30 RPM. Solid mechanics stationary studies were applied to determine Von Mises stresses and Findley's fatigue analysis was applied to determine fatigue of the first study.

In figure 8, the stress on the low-speed shaft is shown, where the maximum stress is in the point load and in the fixed part of the shaft. While in Figure 8b, the deflection of the low-speed shaft is shown, where the maximum deflection occurred at the point load.

Parametric studies were done for the low-speed shaft; table 3 shows the effect of the force on the stress and deflection of the low-speed shaft. It is shown that whenever the force increases, the stress increases for this design and geometry, therefore, the deflection increases. Table 4 shows the effect of the radius on the stress and deflection of the low-speed shaft. It is shown that whenever the radius

increases, the stress decreases due to the increase in the exposed area, therefore, the deflection decreases.

Table. 3: Parametric study for the low speed shaft by changing the force.

Force (N)	RPM	Stress ($\frac{N}{m^2}$)	Deflection (mm)
200	30	2.12E+07	3.038
400	30	4.24E+07	6.076
600	30	6.36E+07	9.113
800	30	8.48E+07	12.151
1000	30	1.06E+08	15.189

Table. 4: Parametric study for the low speed shaft by changing the radius.

Radius (m)	Stress ($\frac{N}{m^2}$)	Deflection (mm)
0.01	1.42E+08	45.69
0.018	2.96E+07	4.61
0.026	1.44E+07	1.13
0.034	6.56E+06	0.41
0.042	5.39E+06	0.20
0.05	2.96E+06	0.10

The fatigue analysis boundary conditions were taken from the studies of solid mechanics (see figure 8c). It is shown that the Findley's fatigue of the low-speed shaft is moderately low. The maximum fatigue of this part occurred at the point load.

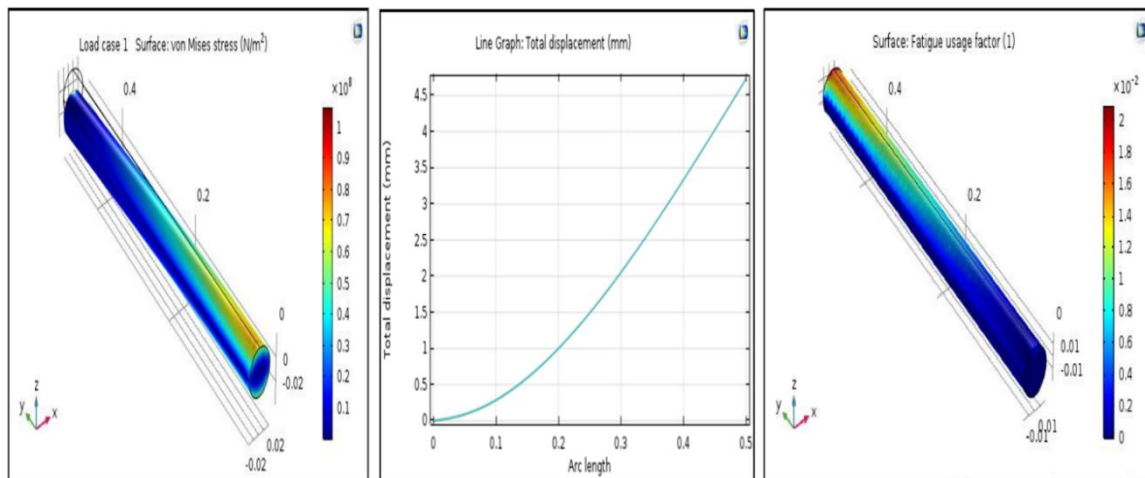


Figure. 8: a. Stress in the low speed shaft, b. Deflection in the low speed shaft and c. Fatigue of the low speed shaft.

3.1. Stationary shaft

The stationary shaft is placed between the hub and the blades. Numerical analysis was applied to determine the Von Mises stresses and fatigue where the shaft was assumed to be a simple design problem of a fixed beam that has a force at the end. The boundary conditions of the low speed shaft are a fixed constraint on the left side of the shaft, a point load on the top right side of the shaft. Solid mechanics stationary studies were applied to determine Von Mises stress and fatigue analyses were applied to determine fatigue of the first study.

In figure 9a, the stress on the stationary shaft is shown, where the maximum stress is in the point load. While in figure 9b, the deflection of the stationary shaft is shown, where the maximum deflection occurred at the point load.

In figure 9c below, the fatigue analysis boundary conditions were taken from the studies of the solid mechanics. It is shown that the Findley's fatigue of the stationary shaft is moderately low. The maximum fatigue of this part occurred at the point load and at the fixed part.

Parametric studies were done for the stationary shaft. Table 5 shows the effect of the force on the stress and deflection of the stationary shaft. It is shown that whenever the force increases, the stress increases, therefore, the deflection increases. Table 6 shows the effect of the radius on the stress and deflection of the stationary shaft. It is shown that whenever the radius increases, the stress decreases, therefore, the deflection decreases. Table. 6: Parametric Study for the Low-Speed Shaft by Changing the Radius.

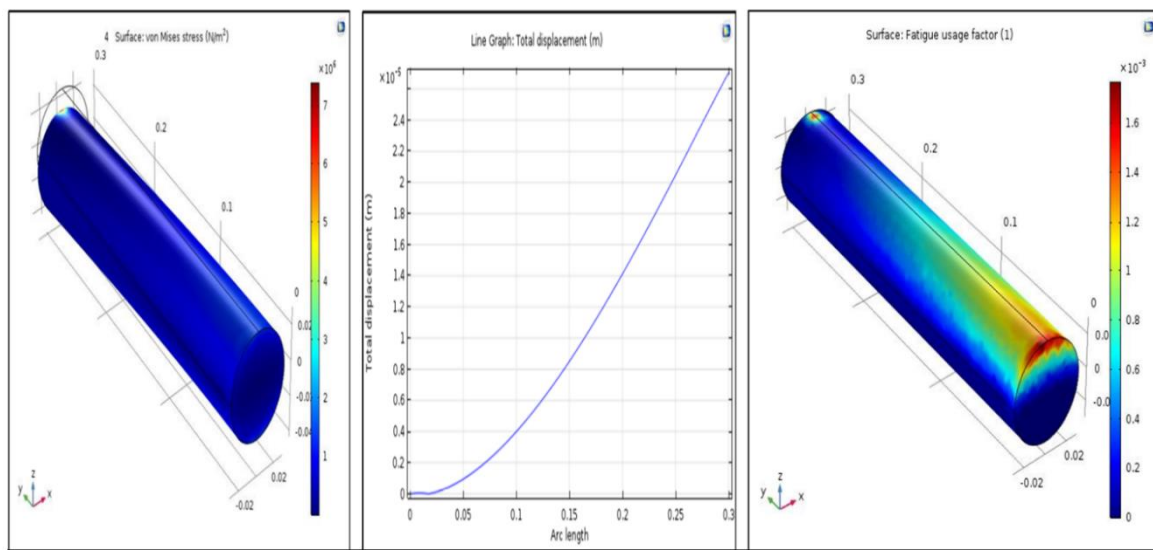


Figure. 9: Stress in the stationary shaft, b. Deflection in the stationary shaft and c. Fatigue in the stationary shaft.

Table.5: Parametric Study for the Stationary Shaft by Changing the Force

Force (N)	Stress ($\frac{N}{m^2}$)	Deflection (mm)
200	1.33E+07	0.34
400	2.65E+07	0.67
600	3.98E+07	1.01
800	5.30E+07	1.34
1000	6.63E+07	1.68

Table. 6: Parametric Study for the Stationary Shaft by Changing the Radius

Radius (m)	Stress ($\frac{N}{m^2}$)	Deflection (mm)
0.01	2.71E+08	35.50
0.02	9.28E+07	3.09
0.03	2.65E+07	0.67
0.04	1.96E+07	0.33
0.05	2.31E+07	0.31

Conclusion

The Magnus wind turbine (MWT) with cylinder blades was modeled by using numerical simulation COMSOL, and aerodynamic characteristics were evaluated. The results of the modeling show that the suggested design of turbine is going to be portable where it can fit into small areas. Also, there is no visible deflection, and the induced stress is less than the allowable limit which points out that the blade is safe, subsequently, no visible deflection is detected which results in no fatigue and this indicates that the low speed shaft, the upper tower, middle and base are safe.

Moreover, the analysis results reveal that the blade can be modeled as a cylinder with built-in support at the end of the hub. A uniformly distributed load is analyzed to represent aerodynamic lift with the high air force. As the force increases, the stress increases, therefore, the deflection increases. The MWT evaluation results illustrate that the radius of the stationary shaft increases, the stress decreases, therefore, the deflection decreases.

Reference

- [1] Abbott. H and Doenhoff. A. E. von. 1959. Theory of Wing Sections. Dover Publications. New York, 326: pp. 113-115.
- [2] AhmedaS. A and Mahammeda. H. O. 2012. A Statistical Analysis of Wind Power Density Based on the Weibull and Rayleigh models of "Penjwen Region" Sulaimani/ Iraq, Jordan Journal of Mechanical and Industrial Engineering, 6(2), pp.135-140.
- [3] AEO. 2017. Annual energy outlook 2017 with projections to 2050.
- [4] Benatiallah. A, Kadi. L , Dakyo. B . 2010. Modelling and Optimisation of Wind Energy Systems, Jordan Journal of Mechanical and Industrial Engineering, 4(1), pp.143-150.
- [5] BORG/ LUTHER group. 1986. The Magnus effect: An overview of its past and future practical applications.
- [6] Cox. D., Davis. C., Ford motor co., Deaborn., MI. 2003. Wind energy: A report prepared for the panel on public affairs (POPA). American physical society William.
- [7] Chantharasanawong. C., Jongpradist. P and Laoharatchapruerk. S. 2011. Preliminary Design of 1.5-MW Modular Wind Turbine Tower. The 2nd TSME International Conference on Mechanical Engineering 19-21 October 2011, Krabi, Thailand.
- [8] Fauzan. M. F., Chelvan. R. K., Amirah. A., 2017. Energy, Economic and Environmental Impact of Wind Power in Malaysia. International Journal of Advanced Scientific Research and Management. 2 (7).
- [9] Ferdous. S., Bin Khaled. W , Ahmed. B., Salehin. S., Ovy. E. 2011. Electric Vehicle with Charging Facility in Motion using Wind Energy. World Rene. Energy congress. 8 -13 may 2011. Linkoping Sweden.
- [10] Ghenai. C , Salameh. T , Janajreh. I.2017. Modeling and Simulation of Shrouded Horizontal Axis Wind Turbine Using RANS Method, Jordan Journal of Mechanical and Industrial Engineering, 11(4), pp.235-243.
- [11] Golding. E. 1976. The generation of electricity by wind power. Halsted press, New York.
- [12] Gregorek. G. M., Hoffmann. M. M., and Berchak. M. J. 1989. Steady State and Oscillatory Aerodynamic Characteristics of a NACA 0021 Airfoil: Data Report, Ohio State University, Columbus, OH.
- [13] Jinbo. M., Farret. F. A., Junior. G. C., Senter. D., Lorensetti. M. F. 2015. MPPT of Magnus Wind System with DC Servo Drive for the Cylinders and Boost Converter. Journal of Wind Energy Volume 2015, Article ID 148680, 10 pages.
- [14] Kaygusuz. K. 2004. Wind Energy: Progress and Potential. Energy Sources, 26:pp. 95–105.
- [15] Khatri. K. K , Sharma. D , Soni. S. L, Kumar. S, Tanwar. D . 2010. Investigation of Optimum Fuel Injection Timing of Direct Injection CI Engine Operated on Preheated Karanj-Diesel Blend. Jordan Journal of Mechanical and Industrial Engineering, 4(5), pp. 629-640.
- [16] Kunz .T.H., Arnett .E.B., Erickson .W.P., Hoar .A.R., Johnson .G.D., et al. 2007. Ecological impacts of wind energy development on bats: questions, research needs, and hypotheses. Frontiers in Ecology and the Environment. 5: pp.315–324.
- [17] Li. H., Hu. Z., Wang. J., Meng. X. 2018. Short-term fatigue analysis for tower base of a spar-type wind turbine under stochastic wind-wave loads. International Journal of Naval Architecture and Ocean Engineering. 10(1):PP. 9- 20.
- [18] Lu. X., McElroy. M. B., Kiviluoma. J. 2009. Global potential for wind-generated electricity. Communicated by James G. Anderson, Harvard University, Cambridge, MA. 106 (27):pp. 10933-10938.
- [19] Minderman. J., Pendlebury .C.J., Pearce-Higgins .J.W., Park .K.J. 2012. Experimental Evidence for the Effect of Small Wind Turbine Proximity and Operation on Bird and Bat Activity. PLOS ONE. 7(7).
- [20] Mayouf Messaoud, Bakhti Hadia , Dahmani Aissab. 2018. Sensorless Control System Design of a Small Size Vertical Axis Wind Turbine, Jordan Journal of Mechanical and Industrial Engineering, 12(2), pp.93-98.
- [21] Messaoud. M and Abdessameda. R. 2011. Modeling and Optimization of Wind Turbine Driving Permanent Magnet Synchronous Generator. Jordan Journal of Mechanical and Industrial Engineering, 5(6), pp.489-44.
- [22] Mishra. S., Purwar. S., Kishor. N. 2017. Maximizing Output Power in Oscillating Water Column Wave Power Plants: An Optimization Based MPPT Algorithm. Technologies. 6(15).
- [23] Musgrove. P.J. 1993. Wind energy conversion- an introduction. IEEE proceeding. 130(9): pp. 506-516.
- [24] Owens. B. 2014. The rise of distributed power.
- [25] Pérez-González. A., Iserte-Vilar. J., González-Lluch. C. 2011. Biomed Eng Online. 2011; 10: 44. Published online 2011 Jun 2. doi: 10.1186/1475-925X-10-44. PMID: PMC3123583.
- [26] Rao. R. S., Mohan.S., G. Kumar. S. 2016. Determination of Fatigue Life of Surface Propeller by Using Finite Element Analysis. IJESC. 6(8).
- [27] Schubel. P.J and Crossley. R. C. 2015. Wind Turbine Blade Design. Energies. 5.
- [28] Seifent. J.2012. A review of the Magnus effect in aeronautics. Progress Aerospace sciences. 55: pp. 17-45.
- [29] Sun. X., Zhuang. Y., Cao. Y., Huang. D., Wu. G. 2012. A three-dimensional numerical study of the Magnus wind turbine with different blade shapes. Journal of Renewable and Sustainable Energy 4(6).
- [30] Tangler. J. 1994. Advanced wind turbine design studies advanced conceptual study final report. NREL. National Technical Information Service.
- [31] Wenchao. L., Luca. S., Harm. A., Fangfang. L., Tianhua. Z.2016. Assessing the integrity of steel structural components with stress raisers using the Theory of Critical Distances. doi: 10.1016/j.engfailanal.2016.07.00.
- [32] WWEA .2012. Small Wind Report 2012. World Wind Energy Association, Bonn, Germany.